

The LISA forecast on a smooth crossover beyond the Standard Model through the scalar-induced gravitational waves

Albert Escrivà,^{1,*} Ryoto Inui,^{1,†} Yuichiro Tada,^{2,1,‡} and Chul-Moon Yoo^{1,§}

¹*Division of Particle and Astrophysical Science, Graduate School of Science, Nagoya University, Nagoya 464-8602, Japan*

²*Institute for Advanced Research, Nagoya University, Furo-cho Chikusa-ku, Nagoya 464-8601, Japan*

(Dated: April 22, 2024)

Supposing the Laser Interferometer Space Antenna (LISA) gravitational wave (GW) detector, we exhibit the detectability of a hypothetical smooth crossover in the early universe beyond the Standard Model of particle physics through the scalar-induced gravitational wave (SIGW) in terms of the Fisher forecast. A crossover at ~ 100 TeV can leave a signal on the GW spectrum in the \sim mHz frequency range, the sweet spot of the LISA sensitivity. These possibilities are also interesting in the primordial black hole (PBH) context as the associated PBH mass $\sim 10^{22}$ g lies at the window to explain the whole dark matter. We found that the properties of the crossover can be well determined if the power spectrum of primordial scalar perturbations are as large as $\sim 5 \times 10^{-4}$ on the corresponding scale $\sim 10^{12}$ Mpc⁻¹.

Introduction.—The Standard Model of particle physics is one of the greatest successes in the history of physics. It unifies all known elementary particles in a mathematically simple way and exhibits high predictability in observables with extraordinary precision represented by the electron’s anomalous magnetic dipole moment [1, 2]. It is, however, true that some phenomena beyond the Standard Model such as the non-zero neutrino mass [3], the baryon asymmetric universe [4], dark matter [5], etc. have been clarified and hence the Standard Model must be improved in these respects. Each hierarchy of physics is often divided by phase transitions or crossovers, as seen in the Standard Model. As in the case of crossovers in the electroweak [6–8] and quantum chromodynamics [9], it may be natural to expect a novel smooth crossover beyond the current energy frontier, e.g., a few TeV or higher.

On the other astrophysical side, the first direct detection of gravitational waves (GWs) by the LIGO collaboration [10] opened a new era to explore physics. The LIGO–Virgo–KAGRA collaborations detected ~ 90 GW events from compact binary coalescences up until the third observing run [11]. In addition, the international pulsar timing array (PTA) networks recently reported the evidence of the stochastic gravitational wave backgrounds (SGWBs) [12–15]. Although their standard interpretation is the superposition of GWs from supermassive black hole binary systems [14–16], they or a part of them can originate from the early universe physics (see, e.g., Refs. [17, 18]), represented by the preheating [19–23], cosmic strings [24–26], bubble collisions at a first-order phase transition [27–30], and so on.

The survey of the effective degrees of freedom of particles in the early universe *through* SGWBs has been also investigated (see, e.g., Refs. [31, 32]). Cosmic inflation is expected to have generated almost scale-invariant SGWBs from the quantum vacuum fluctuations of the tensor modes but their relic spectrum depends on the thermal history of the universe. If some particles get

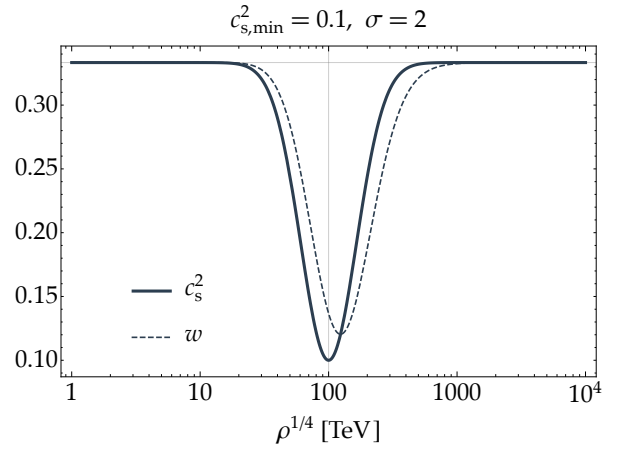


FIG. 1. Illustrations of the modelings of the sound speed squared c_s^2 (1) (black thick) and the EoS parameter w (3) (dashed) for $\rho_*^{1/4} = 100$ TeV (vertical thin), $c_{s,\min}^2 = 0.1$, and $\sigma = 2$. The horizontal thin line indicates the exact radiation value $w = c_s^2 = 1/3$.

massive and become non-relativistic in a hot universe, their pressure reduces and hence the dilution rate of their energy density decreases. Accordingly, the relative energy density of SGWBs to the background energy density decreases. One sees that the equation of motion for GWs (5) indeed depends on the equation-of-state (EoS) parameter $w = p/\rho$ of the background energy density ρ and pressure p . The particle dropout from the thermal plasma is recorded as a *break* of the GW spectrum.

Recently, another type of SGWBs, called the scalar-induced gravitational waves (SIGWs), has attracted attention. The primordial curvature perturbations can source SGWBs through the second-order interaction between the scalar and tensor metric perturbations and could be detected if the scalar curvature perturbations were significantly enhanced compared to the observed value on a cosmological scale (see, e.g., Refs. [33–37]). As

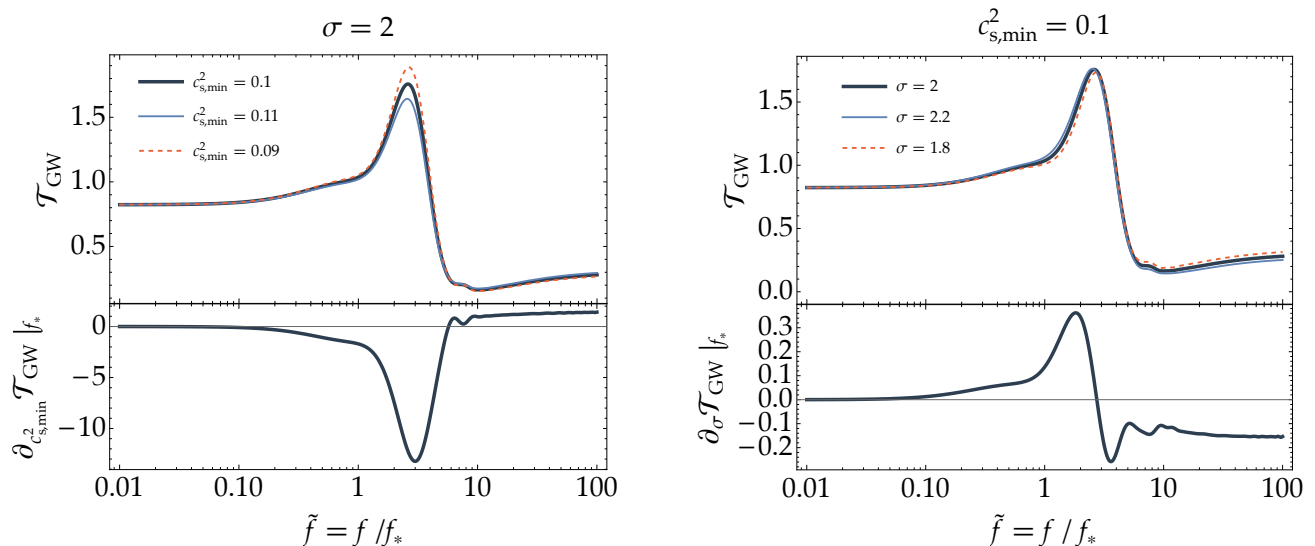


FIG. 2. The numerically-calculated GW template $\mathcal{T}_{\text{GW}}(\tilde{f})$ (11) with varying $c_{\text{s,min}}^2$ (left) and σ (right). The bottom panels show its derivatives in these parameters obtained by the finite difference approximation (15).

the scalar perturbation depends not only on the EoS parameter w but also the plasma sound speed $c_s^2 = \partial p / \partial \rho$, SIGWs are sensitive both on them and helpful to probe the thermal history in more detail (see Refs. [38–42]). Supposing a crossover around ~ 100 TeV beyond Standard Model, the characteristic frequency of the modulated SIGWs reads \sim mHz which is an interesting target of future space-based gravitational wave detectors such as Laser Interferometer Space Antenna (LISA) [43] and DECI-hertz Interferometer Gravitational-wave Observatory (DECIGO) [44, 45], and furthermore large scalar perturbations can bring about the primordial black holes (PBHs) [46–49] (see also Refs. [50–53] for recent review articles) of $\sim 10^{22}$ g as an intriguing candidate of dark matter [42, 54]. In this *Letter*, we want to explicitly show the detectability of that hypothetical smooth crossover beyond the Standard Model in the LISA frequency range. For that purpose, we phenomenologically parameterize the reduction of the sound speed from the relativistic value $c_s^2 = 1/3$ due to a hypothetical crossover as a function of the energy density ρ of the background fluid by (see Fig. 1)

$$c_s^2(\rho) = \frac{1}{3} - \left(\frac{1}{3} - c_{\text{s,min}}^2 \right) \exp \left[- \frac{\ln^2(\rho/\rho_*)}{2\sigma^2} \right], \quad (1)$$

with three model parameters $\boldsymbol{\theta} = (\ln \rho_*^{1/4}, c_{\text{s,min}}^2, \sigma)$ as in Ref. [42], and perform the Fisher forecast on these parameters via SIGWs with the one-year LISA observation, assuming a scale-invariantly amplified scalar power spectrum

$$\mathcal{P}_\zeta(k) = \frac{k^3}{2\pi^2} |\zeta_k|^2 = A_s \gg \mathcal{P}_\zeta(k_{\text{CMB}}) \sim 2 \times 10^{-9}, \quad (2)$$

for the primordial curvature perturbation ζ , for which the change in the spectrum of the induced GWs can be only associated with the effect caused by the crossover. Throughout the *Letter*, we adopt the Planck unit $c = \hbar = G = 1$.

Scalar-induced gravitational waves through a smooth crossover.—Supposing the functional form of c_s^2 as Eq. (1), the consistent EoS parameter is solved as

$$\begin{aligned} w(\rho) &= \frac{1}{\rho} \int_0^{\tilde{\rho}} c_s^2(\tilde{\rho}) d\tilde{\rho} \\ &= \frac{1}{3} - \frac{\sigma}{\rho/\rho_*} \sqrt{\frac{\pi}{2}} e^{\sigma^2/2} \left(\frac{1}{3} - c_{\text{s,min}}^2 \right) \text{erfc} \left[\frac{\sigma^2 - \ln \rho/\rho_*}{\sqrt{2}\sigma} \right], \end{aligned} \quad (3)$$

with the complementary error function $\text{erfc}(z) = \frac{2}{\sqrt{\pi}} \int_z^\infty e^{-t^2} dt$. The background fluid dynamics is fixed by solving the evolution equation for ρ and the Hamiltonian constraint for the scale factor a :

$$\partial_\eta \rho = -\sqrt{24\pi} (1 + w(\rho)) a \rho^{3/2}, \quad \partial_\eta a = \sqrt{\frac{8\pi\rho}{3}} a^2, \quad (4)$$

with the conformal time $\eta = \int a^{-1} dt$. Hereafter, we also use the conformal Hubble parameter defined by $\mathcal{H} = a'/a$ where the prime denotes the derivative in the conformal time.

Over the background evolution, one finds the dynamics of the scalar and tensor perturbations via the equations of motion (see, e.g., Ref. [56]),

$$\begin{aligned} \Phi_k'' + 3\mathcal{H}(1 - c_s^2)\Phi_k' + [c_s^2 k^2 + 3\mathcal{H}^2(c_s^2 - w)]\Phi_k &= 0, \\ \left(\partial_\eta^2 + k^2 - \frac{1 - 3w}{2} \mathcal{H}^2 \right) g_{ik} &= 0, \end{aligned} \quad (5)$$

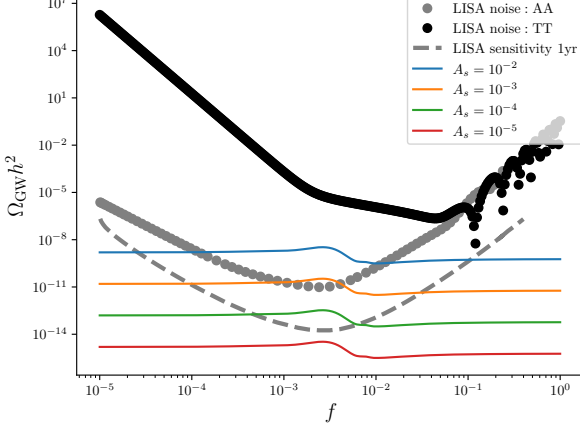


FIG. 3. The GW energy density parameter $\Omega_{\text{GW}}h^2$ and the LISA noise energy density parameters $\Omega_{n,AA}h^2 = \Omega_{n,EE}h^2$ (gray dots) and $\Omega_{n,TT}h^2$ (black dots). The gray dashed line, as a reference, denotes the LISA’s sensitivity for the power-law SIGW assuming one-year observations [55]. The color lines represent the SIGW spectrum for each A_s .

for the scalar transfer function Φ_k and two independent tensor mode functions g_{1k} and g_{2k} . The scalar transfer function should be initialized by $\Phi_k(\eta \rightarrow 0) \sim 1$, while one can take two distinct but arbitrary initial conditions for g_{1k} and g_{2k} such as $g_{1k}(\eta \rightarrow 0) \sim 1$ and $g_{2k}(\eta \rightarrow 0) \sim k\eta$. The power spectrum of SIGWs is calculated in the Green’s function method as

$$\mathcal{P}_h(k, \eta) = \frac{64}{81a^2(\eta)} \int_{|\mathbf{k}_1 - \mathbf{k}_2| \leq k \leq |\mathbf{k}_1 + \mathbf{k}_2|} d \ln k_1 d \ln k_2 I^2(\eta, k_1, k_2, k) \times \frac{(k_1^2 - (k^2 - k_2^2 + k_1^2)^2 / (4k^2))^2}{k_1 k_2 k^2} \mathcal{P}_\zeta(k_1) \mathcal{P}_\zeta(k_2), \quad (6)$$

with the kernel

$$I(\eta, k_1, k_2, k) = k^2 \int^\eta d\tilde{\eta} G_{\mathbf{k}}(\eta, \tilde{\eta}) a(\tilde{\eta}) f(k_1, k_2, \tilde{\eta}), \quad (7)$$

where the tensor Green’s function is given by

$$G_{\mathbf{k}}(\eta, \tilde{\eta}) = \frac{1}{\mathcal{N}_k} [g_{1k}(\eta) g_{2k}(\tilde{\eta}) - g_{1k}(\tilde{\eta}) g_{2k}(\eta)] \Theta(\eta - \tilde{\eta}), \quad (8)$$

with the normalization¹ $\mathcal{N}_k = g'_{1k}(\tilde{\eta}) g_{2k}(\tilde{\eta}) - g_{1k}(\tilde{\eta}) g'_{2k}(\tilde{\eta})$ and the source function reads

$$f(k_1, k_2, \eta) = 2\Phi_{k_1}(\eta) \Phi_{k_2}(\eta) + \frac{4}{3(1-w(\eta))} \left(\Phi_{k_1}(\eta) + \frac{\Phi'_{k_1}(\eta)}{\mathcal{H}(\eta)} \right) \left(\Phi_{k_2}(\eta) + \frac{\Phi'_{k_2}(\eta)}{\mathcal{H}(\eta)} \right). \quad (9)$$

¹ It is indeed time-independent as ensured by the equation of motion (5).

The current GW energy density parameter Ω_{GW} is given by

$$\Omega_{\text{GW}}(k, \eta_0) h^2 = \Omega_{r,0} h^2 \frac{1}{24} \left(\frac{a_c \mathcal{H}_c}{a_f \mathcal{H}_f} \right)^2 \left(\frac{k}{\mathcal{H}_c} \right)^2 \overline{\mathcal{P}_h(k, \eta_c)}, \quad (10)$$

where $\Omega_{r,0}$ is the current radiation energy density parameter, $\Omega_{r,0} h^2 = 4.2 \times 10^{-5}$, with the dimensionless Hubble parameter $h = H_0 / (100 \text{ km s}^{-1} \text{ Mpc}^{-1})$, the subscript “c” denotes the time well after the horizon reentry when the GW density parameter becomes almost constant, and the subscript “f” indicates the time when the degrees of freedom of relativistic species and the entropy are well reduced to the current values after all phase transitions but still in the radiation-dominated era. $\overline{\mathcal{P}_h(k, \eta_c)}$ is the time average of $\mathcal{P}_h(k)$ around η_c within a period of the oscillation. We use the *IGWsfSC* code [57] to numerically compute $\Omega_{\text{GW}}(k, \eta_0)$ through the modeled crossover (1) and (3).

It is useful to make a template as

$$\Omega_{\text{GW}}(f) h^2 = \Omega_{r,0} h^2 A_s^2 \mathcal{T}_{\text{GW}}(\tilde{f}), \quad (11)$$

where the template $\mathcal{T}_{\text{GW}}(\tilde{f})$ should be a function only of the renormalized frequency $\tilde{f} = f/f_*$ with the characteristic frequency $f_* = k_*/(2\pi) = \mathcal{H}_*/(2\pi)$, which corresponds to the Hubble scale at the time when $\rho = \rho_*$. f_* weakly depends also on $c_{s,\text{min}}^2$ and σ through the background equation (4). Supposing $a = 1.93 \times 10^{-17}$ and $\eta = 1.40 \times 10^{-11} \text{ Mpc}$ at $\rho^{1/4} = 10 \text{ TeV}$ to be consistent with the thermal history in the Standard Model and the normalization $a = 1$ today (we have utilized the fitting formulae for effective degrees of freedom given in Ref. [32]), one can numerically find the relation (see Appendix),

$$\frac{f_*}{\text{mHz}} = [c_1 + c_2(c_{s,\text{min}}^2 - 0.1) + c_3(\sigma - 2)] \frac{\rho_*^{1/4}}{100 \text{ TeV}}, \quad (12)$$

with

$$c_1 = 1.019, \quad c_2 = 0.3898, \quad c_3 = -0.0579, \quad (13)$$

around the fiducial values $c_{s,\text{min}}^2 = 0.1$ and $\sigma = 2$. The partial derivative of the GW spectrum in $\rho_*^{1/4}$ fixing $c_{s,\text{min}}^2$ and σ , which is necessary for the Fisher analysis, is equivalent to that in f_* as

$$\left. \frac{\partial_{\ln \rho_*^{1/4}} \Omega_{\text{GW}}(f) h^2}{c_{s,\text{min}}^2, \sigma} \right|_{c_{s,\text{min}}^2, \sigma} = -\Omega_{r,0} h^2 A_s^2 \tilde{f} \mathcal{T}'_{\text{GW}}(\tilde{f}), \quad (14)$$

where $\mathcal{T}'_{\text{GW}}(\tilde{f}) = \partial_{\tilde{f}} \mathcal{T}_{\text{GW}}(\tilde{f})$.

The examples of templates for $c_{s,\text{min}}^2 = 0.1 \pm 0.01$ and $\sigma = 2 \pm 0.2$ are shown in Fig. 2. Such templates with

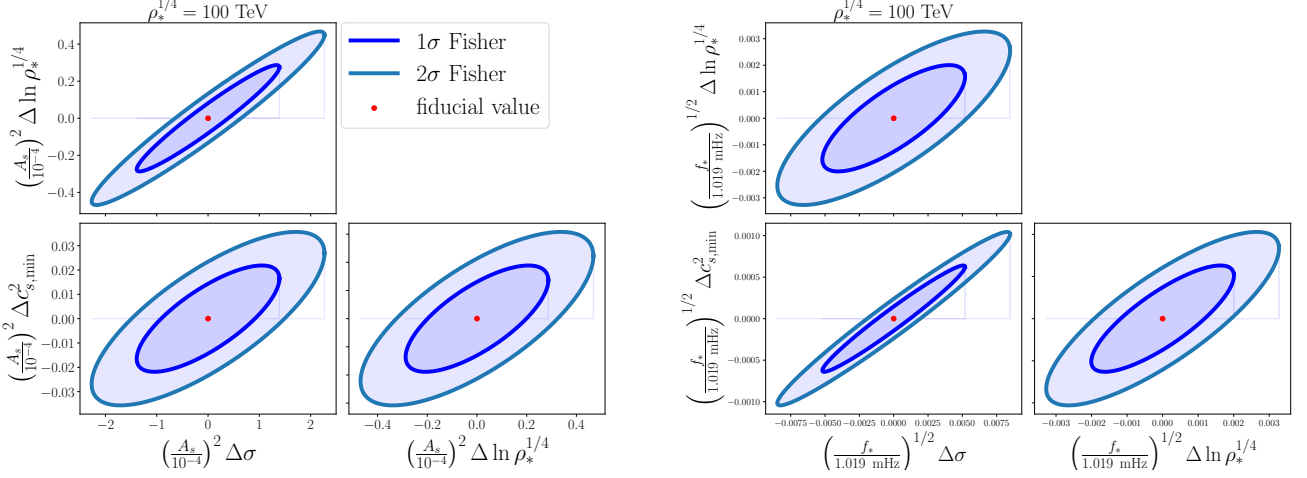


FIG. 4. 1σ (bright blue) and 2σ (pale blue) confidence ranges for the parameter variations $\Delta \ln \rho_*^{1/4}$, $\Delta c_{s,\min}^2$, and $\Delta \sigma$ round the fiducial value $(\rho_*^{1/4}, c_{s,\min}^2, \sigma) = (100 \text{ TeV}, 0.1, 2)$ in the weak limit (18) (left) and the strong limit (19) (right).

slightly shifted parameters around the fiducial values enable us to evaluate other derivatives:

$$\partial_{\theta_i} \mathcal{T}_{\text{GW}}(\tilde{f}) \Big|_{f_*} \approx \frac{\mathcal{T}_{\text{GW}}(\tilde{f} | \theta_i + \Delta \theta_i) - \mathcal{T}_{\text{GW}}(\tilde{f} | \theta_i - \Delta \theta_i)}{2\Delta \theta_i}, \quad (15)$$

for $\theta_2 = c_{s,\min}^2$ and $\theta_3 = \sigma$. Note that, due to the weak dependence of f_* on $c_{s,\min}^2$ and σ , the derivatives fixing ρ_* is contaminated by the derivative in f_* as

$$\partial_{\theta_i} \mathcal{T}_{\text{GW}}(\tilde{f}) \Big|_{\rho_*} = \partial_{\theta_i} \mathcal{T}_{\text{GW}}(\tilde{f}) \Big|_{f_*} - \frac{c_i}{c_1} \tilde{f} \mathcal{T}'_{\text{GW}}(\tilde{f}), \quad (16)$$

for $i = 2$ and 3 .

Fisher analysis in the LISA system.—With the use of the GW spectral derivatives in the model parameters, the Fisher information matrix for SGWBs is calculated as [58–60]

$$F_{ij} = \frac{1}{2} T_{\text{obs}} \sum_I \int_{f_l}^{f_h} df \frac{\partial_{\theta_i} (\Omega_{\text{GW}}(f) h^2) \partial_{\theta_j} (\Omega_{\text{GW}}(f) h^2)}{[\Omega_{n,II}(f) h^2 + \Omega_{\text{GW}}(f) h^2]^2}, \quad (17)$$

where T_{obs} denotes the observational time and $\Omega_{n,II}$ is the noise density spectrum in the independent I channel of the Time Delay Interferometry (TDI) measurement. Explicit expressions for $\Omega_{n,AA} h^2 = \Omega_{n,EE} h^2$ and $\Omega_{n,TT} h^2$ for three independent A , E , and T channels of LISA are given in the Appendix. See Fig. 3 for explicit shapes of the noise density spectra of LISA. The integration range of the Fisher matrix is set to $f_l = 10^{-2} f_*$ and $f_h = 10^2 f_*$. The covariance matrix is given by the inverse of the Fisher matrix (see, e.g., Ref. [61]).

In the weak-signal limit, $\Omega_{\text{GW}} h^2 \ll \Omega_{n,II} h^2$, the parameter dependence of the Fisher matrix can be factor-

ized as

$$F_{ij} \Big|_{\text{weak}} \sim 2.84 \times 10^{21} \left(\frac{T_{\text{obs}}}{1 \text{ yr}} \right) \left(\frac{\Omega_{\text{r}0} h^2}{4.2 \times 10^{-5}} \right)^2 \left(\frac{A_s}{10^{-4}} \right)^4 \times \left(\frac{f_*}{1.019 \text{ mHz}} \right) \sum_I \int_{\tilde{f}_l}^{\tilde{f}_h} d\tilde{f} \frac{\partial_{\theta_i} \mathcal{T}_{\text{GW}}(\tilde{f}) \partial_{\theta_j} \mathcal{T}_{\text{GW}}(\tilde{f})}{(\Omega_{n,II}(\tilde{f} f_*) h^2)^2}, \quad (18)$$

where $\tilde{f}_l = 10^{-2}$ and $\tilde{f}_h = 10^2$. The parameter uncertainties hence scale as $\propto A_s^{-2}$ as expected.² The confidence ellipses are shown in the left panel of Fig. 4 around $(\rho_*^{1/4}, c_{s,\min}^2, \sigma) = (100 \text{ TeV}, 0.1, 2)$ in this limit. While the SIGW is not so sensitive to the crossover smoothness σ in the weak-signal limit, its scale ρ_* and strongness $c_{s,\min}^2$ can be determined at $\sim 10\%$ level for $A_s \sim 10^{-4}$ which is smaller enough than the amplitude required for a sizable PBH formation, $A_s \sim 2 \times 10^{-3}$ [42].

In the strong-signal limit, $\Omega_{\text{GW}} h^2 \gg \Omega_{n,II} h^2$, the Fisher matrix becomes free from the scalar amplitude A_s as well as the detector design and is determined only by the GW template form and the characteristic frequency f_* normalized by the observation time T_{obs} :

$$F_{ij} \Big|_{\text{strong}} \sim 4.82 \times 10^4 \left(\frac{T_{\text{obs}}}{1 \text{ yr}} \right) \left(\frac{f_*}{1.019 \text{ mHz}} \right) \times \int_{\tilde{f}_l}^{\tilde{f}_h} d\tilde{f} \frac{\partial_{\theta_i} \mathcal{T}_{\text{GW}}(\tilde{f}) \partial_{\theta_j} \mathcal{T}_{\text{GW}}(\tilde{f})}{\mathcal{T}_{\text{GW}}^2(\tilde{f})}. \quad (19)$$

The corresponding confidence ellipses are shown in the right panel of Fig. 4. It shows the strongest possible

² Note that the f_* dependence is not simply linear as the noise spectrum depends on f_* in the integral.

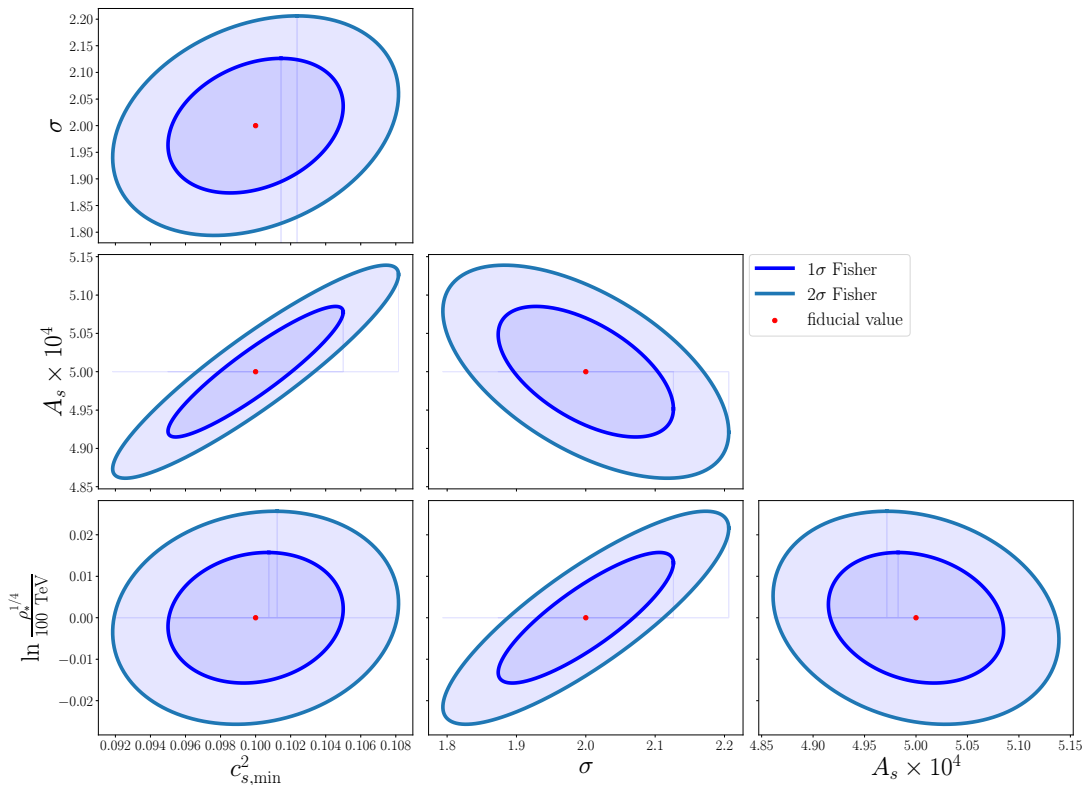


FIG. 5. The marginalized Fisher forecast with the exact expression (17) assuming the one-year observation. The red point denotes the fiducial values, $(c_{s,\min}^2, \sigma, A_s, \rho_*^{1/4}) = (0.1, 2.0, 5 \times 10^{-4}, 100 \text{ TeV})$.

decidability of the crossover parameters with the use of SIGWs irrespective of the GW detector. One can see the significant degeneracy between $c_{s,\min}^2$ and σ , which makes the decidability of each of $c_{s,\min}^2$ and σ worse. As the denominator in the integrand of the Fisher matrix is dominated by the GW spectrum in this limit, the Fisher matrix is sensitive not only to the large- $(\partial_{\theta_i} \mathcal{T}_{\text{GW}})$ part but also to the small- \mathcal{T}_{GW} part. Thus the frequency range much higher than f_* also significantly contributes to the Fisher matrix. Since both the strongness $c_{s,\min}^2$ and the width σ contribute to the reduction of \mathcal{T}_{GW} in the higher frequency range, we find the significant degeneracy in the strong-signal limit. That is, a less significant reduction $\Delta c_{s,\min}^2 > 0$ can be compensated by a longer crossover $\Delta \sigma > 0$ and vice versa.

In Fig. 5, the full confidence ellipses including A_s (note $\partial_{A_s} \Omega_{\text{GW}} h^2 = 2\Omega_{\text{GW}} h^2 / A_s$) are calculated from the exact expression (17) as our main result.

Conclusions.—We exhibited the Fisher forecast on the model parameters of the phenomenological sound-speed reduction (1) in the early universe associated with a certain smooth crossover around 100 TeV beyond the Standard Model of particle physics through the SIGW supposing the one-year LISA observation. The parameter decidability depends on the amplitude A_s of the primordial scalar perturbations around the corresponding scale

$\sim 10^{12} \text{ Mpc}^{-1}$ as a source of SIGWs. The dependence can be inferred by the left (weak A_s limit) and the right (strong A_s limit) of Fig. 4. The main forecast is shown in Fig. 5, indicating that $A_s \sim 5 \times 10^{-4}$ is enough to determine all model parameters.

If the scalar amplitude is slightly higher as $A_s \sim 10^{-3}$, sizable amount of PBHs can be produced at $\sim 10^{22} g$ lying at the observational window for whole dark matters [42, 54]. A significant enough crossover makes the PBH mass function sharp enough to avoid all observational constraints on PBHs even if the scalar power spectrum is almost scale-invariant. Combining our work with this scenario, one can determine not only the crossover parameters but also the abundance of PBHs, as indirect evidence of the nature of dark matter if they are.

We are grateful to Sachiko Kuroyanagi and Javier G. Subils for their helpful discussions. Y.T. is supported by JSPS KAKENHI Grants No. JP21K13918 and JP24K07047. R.I. is supported by JST SPRING, Grant Number JPMJSP2125, and the “Interdisciplinary Frontier Next-Generation Researcher Program of the Tokai Higher Education and Research System”. A.E. acknowledges support from the JSPS Postdoctoral Fellowships for Research in Japan (Graduate School of Sciences, Nagoya University). C.Y. is supported by JSPS KAKENHI Grants No. JP20H05850 and JP20H05853.

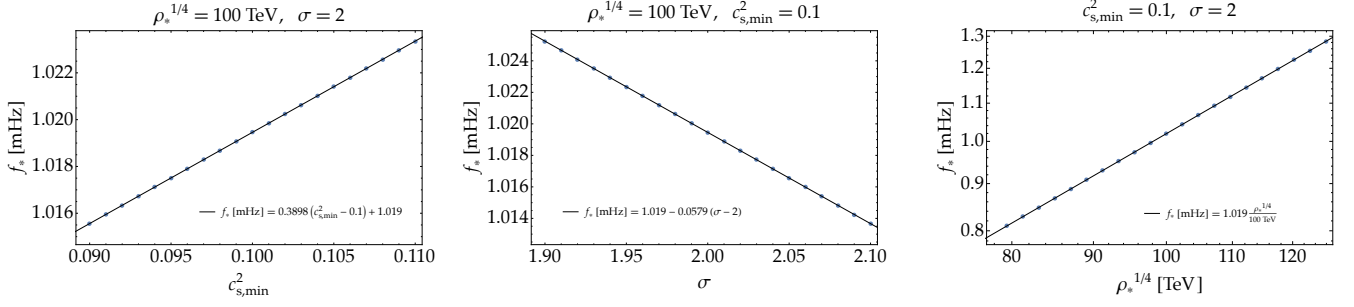


FIG. 6. The f_* dependence on $c_{s,\min}^2$ (left), σ (middle), and ρ_* (right). Blue dots are the numerical results and thin lines are their fitting functions. The fitting formula (12) combines them all.

Crossover scale ρ_* and the characteristic frequency f_*

The characteristic frequency $f_* = k_*/(2\pi) = \mathcal{H}_*/(2\pi)$, where $\mathcal{H}_* = a_*H_*$ is the conformal Hubble parameter at the time when $\rho = \rho_*$, can be found by numerically solving the background equation (4) with the normalization $a = 1$ today. Supposing the standard cosmology in the Standard Model of particle physics is recovered at, e.g., $\rho^{1/4} = 10$ TeV, The normalization can be recast into the condition $a = 1.93 \times 10^{-17}$ and $\eta = 1.40 \times 10^{-11}$ Mpc at $\rho^{1/4} = 10$ TeV with the use of the fitting formulae for effective degrees of freedom given in Ref. [32]. For the fiducial values $(\rho_*^{1/4}, c_{s,\min}^2, \sigma) = (100 \text{ TeV}, 0.1, 2)$, one finds $f_* = 1.019$ mHz.

The f_* dependence on these parameters around the fiducial values can be numerically found by slightly varying the parameters. Fig. 6 shows numerically calculated f_* with shifted parameters as well as their fitting functions. Combining them, one obtains the fitting formula (12).

Noise density parameters of LISA

The noise density parameters of LISA are summarized as [59, 62]

$$\Omega_{n,II}(f)h^2 = \frac{4\pi^2 f^3}{3 \times (100 \text{ km/s/Mpc})^2} \frac{N_{II}(f)}{\mathcal{R}_{II}(f)}, \quad (20)$$

where

$$\begin{aligned} N_{AA}(f) &= N_{EE}(f) \\ &= 8 \sin^2\left(\frac{2\pi fL}{c}\right) \left\{ 4 \left[1 + \cos\left(\frac{2\pi fL}{c}\right) + \cos^2\left(\frac{2\pi fL}{c}\right) \right] P_{\text{acc}}(f) + \left[2 + \cos\left(\frac{2\pi fL}{c}\right) \right] P_{\text{IMS}}(f) \right\}, \\ N_{TT}(f) &= 16 \sin^2\left(\frac{2\pi fL}{c}\right) \left\{ 2 \left[1 - \cos\left(\frac{2\pi fL}{c}\right) \right]^2 P_{\text{acc}}(f) + \left[1 - \cos\left(\frac{2\pi fL}{c}\right) \right] P_{\text{IMS}}(f) \right\}, \end{aligned} \quad (21)$$

and

$$\mathcal{R}_{IJ}(f) = 16 \sin^2\left(\frac{2\pi fL}{c}\right) \left(\frac{2\pi fL}{c}\right)^2 \tilde{\mathcal{R}}_{IJ}(f), \quad (22)$$

with

$$\begin{aligned} P_{\text{IMS}} &= \left(P \text{ pm Hz}^{-1/2} \right)^2 \left[1 + \left(\frac{2 \text{ mHz}}{f} \right)^4 \right] \left(\frac{2\pi f}{c} \right)^2, \\ P_{\text{acc}} &= \left(A \text{ fm s}^{-2} \text{ Hz}^{-1/2} \right)^2 \left[1 + \left(\frac{0.4 \text{ mHz}}{f} \right)^2 \right] \left[1 + \left(\frac{f}{8 \text{ mHz}} \right)^4 \right] \left(\frac{1}{2\pi f} \right)^4 \left(\frac{2\pi f}{c} \right)^2, \end{aligned} \quad (23)$$

and

$$\tilde{R}_{AA}(f) = \tilde{R}_{EE}(f) = \frac{9}{20} \frac{1}{1 + 0.7 \left(\frac{2\pi fL}{c}\right)^2}, \quad \tilde{R}_{TT}(f) = \frac{9}{20} \frac{\left(\frac{2\pi fL}{c}\right)^6}{1.8 \times 10^3 + 0.7 \left(\frac{2\pi fL}{c}\right)^8}. \quad (24)$$

We explicitly show the speed of light c for clarity. The dominant noise components of the LISA system are the position noise so-called the Interferometry Metrology System (IMS) due to laser shot noise and the acceleration noise raised from internal sensors. $P = 15$ and $A = 3$ are chosen for the noise power (23), following Refs. [59, 62].

* escriva.manas.albert.y0@a.mail.nagoya-u.ac.jp

† inui.ryoto.a3@s.mail.nagoya-u.ac.jp

‡ tada.yuichiro.y8@f.mail.nagoya-u.ac.jp

§ yoo.chulmoon.k6@f.mail.nagoya-u.ac.jp

- [1] P. Kusch and H. M. Foley, The Magnetic Moment of the Electron, *Phys. Rev.* **74**, 250 (1948).
- [2] J. S. Schwinger, On Quantum electrodynamics and the magnetic moment of the electron, *Phys. Rev.* **73**, 416 (1948).
- [3] Y. Fukuda *et al.* (Super-Kamiokande), Evidence for oscillation of atmospheric neutrinos, *Phys. Rev. Lett.* **81**, 1562 (1998), [arXiv:hep-ex/9807003](https://arxiv.org/abs/hep-ex/9807003).
- [4] A. D. Sakharov, Violation of CP Invariance, C asymmetry, and baryon asymmetry of the universe, *Pisma Zh. Eksp. Teor. Fiz.* **5**, 32 (1967).
- [5] F. Zwicky, Die Rotverschiebung von extragalaktischen Nebeln, *Helvetica Physica Acta* **6**, 110 (1933).
- [6] K. Kajantie, M. Laine, K. Rummukainen, and M. E. Shaposhnikov, Is there a hot electroweak phase transition at $m_H \gtrsim m_W$?, *Phys. Rev. Lett.* **77**, 2887 (1996), [arXiv:hep-ph/9605288](https://arxiv.org/abs/hep-ph/9605288).
- [7] M. Laine and K. Rummukainen, A Strong electroweak phase transition up to $m(H)$ is about 105-GeV, *Phys. Rev. Lett.* **80**, 5259 (1998), [arXiv:hep-ph/9804255](https://arxiv.org/abs/hep-ph/9804255).
- [8] K. Rummukainen, M. Tsypin, K. Kajantie, M. Laine, and M. E. Shaposhnikov, The Universality class of the electroweak theory, *Nucl. Phys. B* **532**, 283 (1998), [arXiv:hep-lat/9805013](https://arxiv.org/abs/hep-lat/9805013).
- [9] Y. Aoki, G. Endrodi, Z. Fodor, S. D. Katz, and K. K. Szabo, The Order of the quantum chromodynamics transition predicted by the standard model of particle physics, *Nature* **443**, 675 (2006), [arXiv:hep-lat/0611014](https://arxiv.org/abs/hep-lat/0611014).
- [10] B. P. Abbott *et al.* (LIGO Scientific, Virgo), Observation of Gravitational Waves from a Binary Black Hole Merger, *Phys. Rev. Lett.* **116**, 061102 (2016), [arXiv:1602.03837](https://arxiv.org/abs/1602.03837) [gr-qc].
- [11] R. Abbott *et al.* (KAGRA, VIRGO, LIGO Scientific), GWTC-3: Compact Binary Coalescences Observed by LIGO and Virgo during the Second Part of the Third Observing Run, *Phys. Rev. X* **13**, 041039 (2023), [arXiv:2111.03606](https://arxiv.org/abs/2111.03606) [gr-qc].
- [12] G. Agazie *et al.* (NANOGrav), The NANOGrav 15 yr Data Set: Evidence for a Gravitational-wave Background, *Astrophys. J. Lett.* **951**, L8 (2023), [arXiv:2306.16213](https://arxiv.org/abs/2306.16213) [astro-ph.HE].
- [13] J. Antoniadis *et al.* (EPTA, InPTA:), The second data release from the European Pulsar Timing Array - III. Search for gravitational wave signals, *Astron. Astrophys.* **678**, A50 (2023), [arXiv:2306.16214](https://arxiv.org/abs/2306.16214) [astro-ph.HE].
- [14] D. J. Reardon *et al.*, Search for an Isotropic Gravitational-wave Background with the Parkes Pulsar Timing Array, *Astrophys. J. Lett.* **951**, L6 (2023), [arXiv:2306.16215](https://arxiv.org/abs/2306.16215) [astro-ph.HE].
- [15] H. Xu *et al.*, Searching for the Nano-Hertz Stochastic Gravitational-wave Background with the Chinese Pulsar Timing Array Data Release I, *Res. Astron. Astrophys.* **23**, 075024 (2023), [arXiv:2306.16216](https://arxiv.org/abs/2306.16216) [astro-ph.HE].
- [16] J. Antoniadis *et al.*, The International Pulsar Timing Array second data release: Search for an isotropic gravitational wave background, *Mon. Not. Roy. Astron. Soc.* **510**, 4873 (2022), [arXiv:2201.03980](https://arxiv.org/abs/2201.03980) [astro-ph.HE].
- [17] A. Afzal *et al.* (NANOGrav), The NANOGrav 15 yr Data Set: Search for Signals from New Physics, *Astrophys. J. Lett.* **951**, L11 (2023), [arXiv:2306.16219](https://arxiv.org/abs/2306.16219) [astro-ph.HE].
- [18] J. Antoniadis *et al.* (EPTA), The second data release from the European Pulsar Timing Array: V. Implications for massive black holes, dark matter and the early Universe, [arXiv:2306.16227](https://arxiv.org/abs/2306.16227) [astro-ph.CO] (2023).
- [19] A. A. Starobinsky, Spectrum of relict gravitational radiation and the early state of the universe, *JETP Lett.* **30**, 682 (1979).
- [20] M. S. Turner, Detectability of inflation produced gravitational waves, *Phys. Rev. D* **55**, R435 (1997), [arXiv:astro-ph/9607066](https://arxiv.org/abs/astro-ph/9607066).
- [21] S. Y. Khlebnikov and I. I. Tkachev, Relic gravitational waves produced after preheating, *Phys. Rev. D* **56**, 653 (1997), [arXiv:hep-ph/9701423](https://arxiv.org/abs/hep-ph/9701423).
- [22] J. Garcia-Bellido, D. G. Figueroa, and A. Sastre, A Gravitational Wave Background from Reheating after Hybrid Inflation, *Phys. Rev. D* **77**, 043517 (2008), [arXiv:0707.0839](https://arxiv.org/abs/0707.0839) [hep-ph].
- [23] N. Aggarwal *et al.*, Challenges and opportunities of gravitational-wave searches at MHz to GHz frequencies, *Living Rev. Rel.* **24**, 4 (2021), [arXiv:2011.12414](https://arxiv.org/abs/2011.12414) [gr-qc].
- [24] B. P. Abbott *et al.* (LIGO Scientific, Virgo), Constraints on cosmic strings using data from the first Advanced LIGO observing run, *Phys. Rev. D* **97**, 102002 (2018), [arXiv:1712.01168](https://arxiv.org/abs/1712.01168) [gr-qc].
- [25] R. Abbott *et al.* (LIGO Scientific, Virgo, KAGRA), Constraints on Cosmic Strings Using Data from the Third Advanced LIGO–Virgo Observing Run, *Phys. Rev. Lett.* **126**, 241102 (2021), [arXiv:2101.12248](https://arxiv.org/abs/2101.12248) [gr-qc].
- [26] N. van Remortel, K. Janssens, and K. Turbang, Stochastic gravitational wave background: Methods and implications, *Prog. Part. Nucl. Phys.* **128**, 104003 (2023), [arXiv:2210.00761](https://arxiv.org/abs/2210.00761) [gr-qc].
- [27] E. Witten, Cosmic Separation of Phases, *Phys. Rev. D* **30**, 272 (1984).
- [28] A. Kosowsky, M. S. Turner, and R. Watkins, Gravita-

- tional radiation from colliding vacuum bubbles, *Phys. Rev. D* **45**, 4514 (1992).
- [29] A. Kosowsky and M. S. Turner, Gravitational radiation from colliding vacuum bubbles: envelope approximation to many bubble collisions, *Phys. Rev. D* **47**, 4372 (1993), [arXiv:astro-ph/9211004](#).
- [30] C. Caprini and D. G. Figueroa, Cosmological Backgrounds of Gravitational Waves, *Class. Quant. Grav.* **35**, 163001 (2018), [arXiv:1801.04268 \[astro-ph.CO\]](#).
- [31] S. Kuroyanagi, T. Chiba, and N. Sugiyama, Precision calculations of the gravitational wave background spectrum from inflation, *Phys. Rev. D* **79**, 103501 (2009), [arXiv:0804.3249 \[astro-ph\]](#).
- [32] K. Saikawa and S. Shirai, Primordial gravitational waves, precisely: The role of thermodynamics in the Standard Model, *JCAP* **05**, 035, [arXiv:1803.01038 \[hep-ph\]](#).
- [33] K. N. Ananda, C. Clarkson, and D. Wands, The Cosmological gravitational wave background from primordial density perturbations, *Phys. Rev. D* **75**, 123518 (2007), [arXiv:gr-qc/0612013](#).
- [34] D. Baumann, P. J. Steinhardt, K. Takahashi, and K. Ichiki, Gravitational Wave Spectrum Induced by Primordial Scalar Perturbations, *Phys. Rev. D* **76**, 084019 (2007), [arXiv:hep-th/0703290](#).
- [35] R. Saito and J. Yokoyama, Gravitational wave background as a probe of the primordial black hole abundance, *Phys. Rev. Lett.* **102**, 161101 (2009), [Erratum: *Phys.Rev.Lett.* 107, 069901 (2011)], [arXiv:0812.4339 \[astro-ph\]](#).
- [36] K. Kohri and T. Terada, Semianalytic calculation of gravitational wave spectrum nonlinearly induced from primordial curvature perturbations, *Phys. Rev. D* **97**, 123532 (2018), [arXiv:1804.08577 \[gr-qc\]](#).
- [37] G. Domènech, Scalar Induced Gravitational Waves Review, *Universe* **7**, 398 (2021), [arXiv:2109.01398 \[gr-qc\]](#).
- [38] F. Hajkarim and J. Schaffner-Bielich, Thermal History of the Early Universe and Primordial Gravitational Waves from Induced Scalar Perturbations, *Phys. Rev. D* **101**, 043522 (2020), [arXiv:1910.12357 \[hep-ph\]](#).
- [39] G. Domènech, S. Pi, and M. Sasaki, Induced gravitational waves as a probe of thermal history of the universe, *JCAP* **08**, 017, [arXiv:2005.12314 \[gr-qc\]](#).
- [40] K. T. Abe, Y. Tada, and I. Ueda, Induced gravitational waves as a cosmological probe of the sound speed during the QCD phase transition, *JCAP* **06**, 048, [arXiv:2010.06193 \[astro-ph.CO\]](#).
- [41] K. T. Abe and Y. Tada, Translating nano-Hertz gravitational wave background into primordial perturbations taking account of the cosmological QCD phase transition, *Phys. Rev. D* **108**, L101304 (2023), [arXiv:2307.01653 \[astro-ph.CO\]](#).
- [42] A. Escrivà, Y. Tada, and C.-M. Yoo, Primordial Black Holes and Induced Gravitational Waves from a Smooth Crossover beyond Standard Model, [arXiv:2311.17760 \[astro-ph.CO\]](#) (2023).
- [43] P. Amaro-Seoane *et al.* (LISA), Laser Interferometer Space Antenna, [arXiv:1702.00786 \[astro-ph.IM\]](#) (2017).
- [44] N. Seto, S. Kawamura, and T. Nakamura, Possibility of direct measurement of the acceleration of the universe using 0.1-Hz band laser interferometer gravitational wave antenna in space, *Phys. Rev. Lett.* **87**, 221103 (2001), [arXiv:astro-ph/0108011](#).
- [45] S. Kawamura *et al.*, The Japanese space gravitational wave antenna: DECIGO, *Class. Quant. Grav.* **28**, 094011 (2011).
- [46] Y. B. Zel'dovich and I. D. Novikov, The Hypothesis of Cores Retarded during Expansion and the Hot Cosmological Model, *Sov. Astron.* **10**, 602 (1967).
- [47] S. Hawking, Gravitationally collapsed objects of very low mass, *Mon. Not. Roy. Astron. Soc.* **152**, 75 (1971).
- [48] B. J. Carr and S. W. Hawking, Black holes in the early Universe, *Mon. Not. Roy. Astron. Soc.* **168**, 399 (1974).
- [49] B. J. Carr, The Primordial black hole mass spectrum, *Astrophys. J.* **201**, 1 (1975).
- [50] B. Carr, K. Kohri, Y. Sendouda, and J. Yokoyama, Constraints on primordial black holes, *Rept. Prog. Phys.* **84**, 116902 (2021), [arXiv:2002.12778 \[astro-ph.CO\]](#).
- [51] A. Escrivà, F. Kuhnel, and Y. Tada, Primordial Black Holes, [arXiv:2211.05767 \[astro-ph.CO\]](#) (2022).
- [52] C.-M. Yoo, The Basics of Primordial Black Hole Formation and Abundance Estimation, *Galaxies* **10**, 112 (2022), [arXiv:2211.13512 \[astro-ph.CO\]](#).
- [53] B. Carr, S. Clesse, J. Garcia-Bellido, M. Hawkins, and F. Kuhnel, Observational evidence for primordial black holes: A positivist perspective, *Phys. Rept.* **1054**, 1 (2024), [arXiv:2306.03903 \[astro-ph.CO\]](#).
- [54] A. Escrivà and J. G. Subils, Primordial black hole formation during a strongly coupled crossover, *Phys. Rev. D* **107**, L041301 (2023), [arXiv:2211.15674 \[astro-ph.CO\]](#).
- [55] K. Schmitz, New Sensitivity Curves for Gravitational-Wave Signals from Cosmological Phase Transitions, *JHEP* **01**, 097, [arXiv:2002.04615 \[hep-ph\]](#).
- [56] V. Mukhanov, *Physical Foundations of Cosmology* (Cambridge University Press, Oxford, 2005).
- [57] IGWsfSC code, <https://github.com/albert-escriva/IGWsfSC.git> (2024), [Online].
- [58] M. Tegmark, A. Taylor, and A. Heavens, Karhunen-Loeve eigenvalue problems in cosmology: How should we tackle large data sets?, *Astrophys. J.* **480**, 22 (1997), [arXiv:astro-ph/9603021](#).
- [59] T. L. Smith, T. L. Smith, R. R. Caldwell, and R. Caldwell, LISA for Cosmologists: Calculating the Signal-to-Noise Ratio for Stochastic and Deterministic Sources, *Phys. Rev. D* **100**, 104055 (2019), [Erratum: *Phys.Rev.D* 105, 029902 (2022)], [arXiv:1908.00546 \[astro-ph.CO\]](#).
- [60] G. Boileau, A. C. Jenkins, M. Sakellariadou, R. Meyer, and N. Christensen, Ability of LISA to detect a gravitational-wave background of cosmological origin: The cosmic string case, *Phys. Rev. D* **105**, 023510 (2022), [arXiv:2109.06552 \[gr-qc\]](#).
- [61] D. Coe, Fisher Matrices and Confidence Ellipses: A Quick-Start Guide and Software, [arXiv:0906.4123 \[astro-ph.IM\]](#) (2009).
- [62] R. Flauger, N. Karnesis, G. Nardini, M. Pieroni, A. Ricciardone, and J. Torrado, Improved reconstruction of a stochastic gravitational wave background with LISA, *JCAP* **01**, 059, [arXiv:2009.11845 \[astro-ph.CO\]](#).